Protein Science (1998), 7:545–555. Cambridge University Press. Printed in the USA.

Subunit asymmetry in the three-dimensional structure of a human CuZnSOD mutant found in familial amyotrophic lateral sclerosis

P. JOHN HART,[1,2] HONGBIN LIU,[2] MATTEO PELLEGRINI,[2] ARAM M. NERSISSIAN,[2] EDITH B. GRALLA,[2] JOAN S. VALENTINE,[2] AND DAVID EISENBERG[1–3]

[1]UCLA-DOE Laboratory of Structural Biology and Molecular Medicine, University of California, Los Angeles, California 90095
[2]Department of Chemistry and Biochemistry, University of California, Los Angeles, California 90095
[3]Department of Biological Chemistry, University of California, Los Angeles, California 90095

(RECEIVED September 23, 1997; ACCEPTED December 2, 1997)

Abstract

The X-ray crystal structure of a human copper/zinc superoxide dismutase mutant (G37R CuZnSOD) found in some patients with the inherited form of Lou Gehrig's disease (FALS) has been determined to 1.9 Å resolution. The two SOD subunits have distinct environments in the crystal and are different in structure at their copper binding sites. One subunit ($subunit_{intact}$) shows a four-coordinate ligand geometry of the copper ion, whereas the other subunit ($subunit_{broken}$) shows a three-coordinate geometry of the copper ion. Also, $subunit_{intact}$ displays higher atomic displacement parameters for backbone atoms ($\langle B \rangle = 30 \pm 10$ Å^2) than $subunit_{broken}$ ($\langle B \rangle = 24 \pm 11$ Å^2). This structure is the first CuZnSOD to show large differences between the two subunits. Factors that may contribute to these differences are discussed and a possible link of a looser structure to FALS is suggested.

Keywords: amyotrophic lateral sclerosis; apoptosis; Lou Gehrig's disease; motor neuron; neurodegeneration; oxidative damage; superoxide dismutase; X-ray crystallography

Human CuZnSOD is a 32-kDa metalloprotein encoded by the *SOD1* gene. *SOD1* lies on chromosome 21, consists of five small exons, and encodes a 153-amino acid protein (Levanon et al., 1985). Two such monomers associate into the functional 306-amino acid homodimer exhibiting an extensive (~845 Å^2/monomer) interface stabilized by apolar, hydrogen bonding, and water-mediated interactions. Each monomer binds one copper and one zinc ion and displays the Greek key β-barrel folding topology.

CuZnSOD provides cellular defense against oxidative damage by catalyzing the disproportionation of superoxide into dioxygen and hydrogen peroxide ($2O_2^- + 2H^+ \rightarrow O_2 + H_2O_2$) (Fridovich, 1989). The widely accepted enzymatic mechanism for CuZnSOD involves alternating reduction of the oxidized Cu(II) form of the enzyme by superoxide, producing dioxygen (reaction 1), and oxidation of the reduced Cu(I) form by another superoxide, producing hydrogen peroxide (reaction 2) (Rotilio et al., 1971, 1972; Klug-Roth et al., 1973; Fielden et al., 1974).

$$O_2^- + \text{Cu(II)ZnSOD} \rightarrow O_2 + \text{Cu(I)ZnSOD} \quad (1)$$

$$O_2^- + \text{Cu(I)ZnSOD} + 2H^+ \rightarrow H_2O_2 + \text{Cu(II)ZnSOD}. \quad (2)$$

In the Cu(II) form of the enzyme, crystallographic and spectroscopic studies have shown that a histidyl residue (His 63 in human) simultaneously coordinates the copper and zinc ions. This histidine residue, termed the "histidine bridge" or "bridging imidazolate" is unique to CuZnSOD. The copper-binding geometry in the oxidized protein has been described as distorted square planar, with histidine residues 46, 48, 63, and 120 acting as ligands in the human protein (Valentine & Pantoliano, 1981; Tainer et al., 1982, 1983; Bertini et al., 1985, 1990; Bannister et al., 1987; Kitagawa et al., 1991; Djinovic et al., 1992; Djinovic-Carugo et al., 1994). In the Cu(I) form of the enzyme, crystallographic and spectroscopic analyses revealed that the bridging imidazolate is protonated on the copper-binding side at its NE2 atom. The loss of the His 63-Cu bond upon copper reduction results in a nearly trigonal-planar copper coordination geometry with histidine residues 46, 48, and 120 acting as ligands (Blackburn et al., 1984; Bertini et al., 1985; Banci et al., 1994; Ogihara et al., 1996; Murphy et al., 1997). It should be noted, however, that a recent crystallographic study on the Cu(I) form of the bovine enzyme revealed no indication of the imidazolate bridge being broken between the copper and zinc ions (Rypniewski et al., 1995).

Reprint requests to: David Eisenberg, Molecular Biology Institute, University of California Los Angeles, Box 951570, Los Angeles, California 90095; e-mail: david@pauling.mbi.ucla.edu.

Abbreviations: FALS, familial amyotrophic lateral sclerosis; CuZnSOD, copper/zinc superoxide dismutase; G37R, glycine to arginine mutation in human CuZnSOD; RMSD, RMS deviation; *SOD1*, gene encoding human copper/zinc superoxide dismutase.

CuZnSOD is present in the cytoplasm of most cells, and is particularly abundant in red blood cells and in neurons (~1% mass of spinal tissue protein) (Pardo et al., 1995; Wong et al., 1995). Superoxide is guided to the copper-containing active site by a conserved set of charged amino acid residues (Tainer et al., 1988; Getzoff et al., 1989, 1992). The active-site channel containing these charges narrows from a shallow depression about 24 Å across to a deeper channel about 10 Å wide, and finally to an opening of less than 4 Å just above the Cu atom. Access to the active site is limited to small negatively charged ions (Tainer et al., 1988).

The SOD-FALS connection

Amyotrophic lateral sclerosis, also known as Lou Gehrig's disease, is a neurodegenerative disorder characterized by the destruction of large motor neurons in the spinal cord and brain. The disease results in a progressive paralysis, typically culminating in the death of the afflicted person within two to five years of symptom onset (Haverkamp et al., 1995). Approximately 5–10% of cases are familial (Juneja et al., 1997), and approximately 15–25% of familial ALS cases are associated with dominantly inherited mutations in *SOD1* (Cudkowicz & Brown, 1996; Juneja et al., 1997).

Initially, 11 different missense mutations in 13 different FALS families were identified (Rosen et al., 1993). These were found to cluster in regions thought critical for maintaining the three-dimensional architecture of the human CuZnSOD protein, namely at the homodimer interface and in loop regions at the ends of β-strands (Deng et al., 1993).

By 1997, the number of distinct FALS mutations identified had risen to about 50 (Siddique & Deng, 1996; Juneja et al., 1997). Although there is still a clustering of mutant residues at the homodimer interface and in loop regions at the ends of β-strands, it is now clear that in FALS, the human CuZnSOD molecule is affected in a global sense. The more recently identified FALS mutations are found to map to many regions of the molecule, including the β-strands and two of the copper-liganding residues (H46R and H48Q) (Aoki et al., 1994; Carri et al., 1994; Enayat et al., 1995). *SOD1* mutations identified in FALS are present in all exons. Five different mutations are seen in codon 93 of exon 4. The G37R mutation is found in exon 2. Figure 1A illustrates the distribution of the FALS mutated residues on the known structure of the wild-type human CuZnSOD molecule (1spd) (Deng et al., 1993) and highlights the position of the G37R mutation.

The mechanism(s) by which single amino acid changes in the SOD molecule lead to FALS are not yet understood. Diverse ideas have been presented, ranging from decreased enzymatic activity (Deng et al., 1993) to an acquired gain of function, such as nonspecific peroxidation (Hodgson & Fridovich, 1975; Cabelli et al., 1989; Wiedau-Pazos et al., 1996; Yim et al., 1996, 1997) or nitration of critical cellular constituents (see below) (Beckman et al., 1992, 1993). Recent studies support the nonspecific peroxidation hypothesis by demonstrating that two of the human FALS mutants, A4V and G93A, catalyze the oxidation of a model substrate by hydrogen peroxide at higher rates than that seen with the wild-type enzyme (Wiedau-Pazos et al., 1996; Yim et al., 1996, 1997). This fact in turn suggests the hypothesis that oxidative reactions catalyzed by mutant human SODs initiate the neuropathologic changes associated with FALS (Wiedau-Pazos et al., 1996; Yim et al., 1996, 1997).

Beckman et al. (1992, 1993) have proposed that an abnormal CuZnSOD protein with unusually accessible (or less tightly bound) copper may have an enhanced capacity to react with peroxynitrite ($ONOO^-$), formed from the reaction of superoxide (O_2^-) with nitric oxide (NO) in vivo. This in turn might lead to the formation of nitronium ions and nitration of tyrosine residues in vulnerable proteins, such as tyrosine kinase receptors (Beckman et al., 1992, 1993; Ischiropoulos et al., 1992).

Compelling evidence that FALS mutations play a direct role in the onset of neurodegenerative disease (by whatever mechanism) comes from studies of transgenic mouse. Transgenic mice expressing excess human wild-type CuZnSOD have been shown to grow and live without obvious serious deleterious effects (Epstein et al., 1987; Dal Canto & Gurney, 1995). Surprisingly, CuZnSOD knockout mice (SOD^-) also appear normal, at least for the first six months of life, unless they are subjected to axonal injury (Reaume et al., 1996). On the other hand, transgenic mice expressing FALS mutant CuZnSODs in addition to their own normal CuZnSOD (and therefore having higher than normal CuZnSOD activity) develop motor neuron disease (Gurney et al., 1994; Pardo et al., 1995; Ripps et al., 1995; Wong et al., 1995).

G37R CuZnSOD

The G37R FALS mutant CuZnSOD protein exhibits the following characteristics. (1) G37R retains full specific activity both in vitro and in patient samples (Borchelt et al., 1994). (2) G37R displays approximate twofold reduction in polypeptide stability relative to wild type (Borchelt et al., 1994). (3) Mice expressing human G37R CuZnSOD at 4–12 times the normal level of mouse *SOD1* (resulting in a corresponding 5–14-fold elevation in normal *SOD1* activity levels) develop classic, progressive motor neuron disease with onset between age 4 and 6 months (Cleveland et al., 1996). (4) Mice expressing human G37R CuZnSOD exhibit two- to threefold elevation in free nitrotyrosine levels in spinal cord tissue relative to normal mice or mice expressing high levels of wild-type human enzyme (Bruijn et al., 1997). (5) Although expression of wild-type

Fig. 1 (*facing page*). **A:** Human CuZnSOD homodimer with FALS mutations. The molecular twofold axis is horizontal in the plane of the paper. Protein backbone is represented as a gray coil, positions of the currently known FALS mutations as red ball-and-stick β-carbons, copper and zinc ions as blue and yellow spheres, respectively, and the G37R mutation as green ball-and-stick side chains. **B:** Human CuZnSOD wild-type superimposed on G37R FALS mutant. This view is in the same orientation as in A. Human wild-type CuZnSOD backbone is shown as a purple coil, the G37R FALS mutant backbone as a gray coil, copper and zinc ions as blue and yellow spheres, respectively, and the G37R mutation as red ball-and-stick side chains. Main-chain atoms superimpose with an RMSD of 0.90 Å. **C:** Superposition of G37R FALS mutant CuZnSOD monomers. This view is as in A and B for the top monomer, but rotated ~90° around an axis coming out of the plane of the paper. $Subunit_{intact}$ and $subunit_{broken}$ (see text) are represented as black and gray coils, respectively. Copper and zinc ions are represented as blue and yellow spheres, respectively. Position of the G37R mutation is shown as a red ball-and-stick β-carbon. Main-chain atoms superimpose with an RMSD of 0.21 Å.

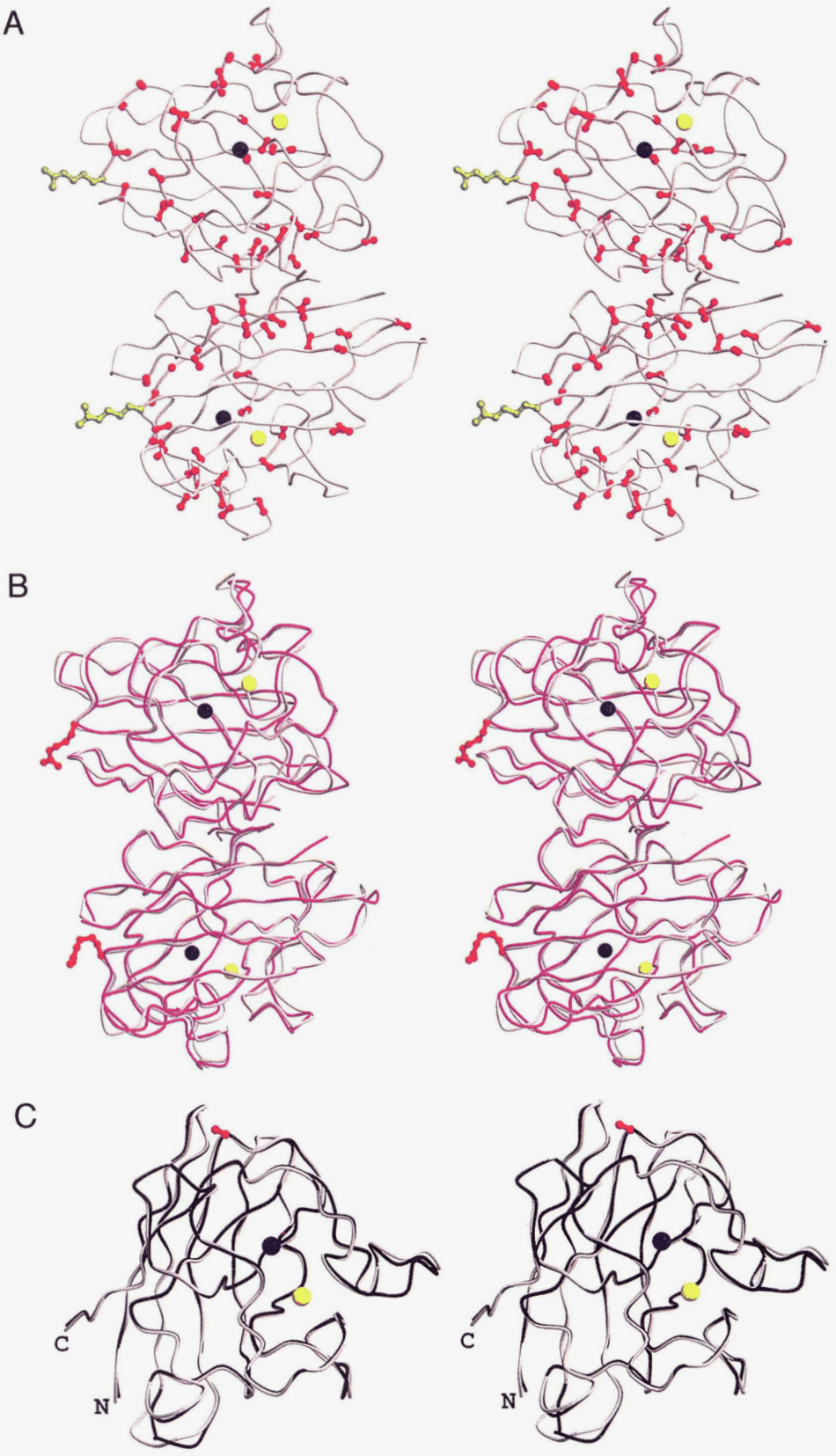
A
B
C
C
N
C
N

human CuZnSOD in neural cell lines inhibits apoptosis, the expression of the FALS mutants A4V and G37R enhance apoptosis in a dominant fashion, despite increasing SOD activity to nearly the wild-type level (Rabizadeh et al., 1995).

Structural studies of FALS CuZnSOD mutants

X-ray crystallography offers the opportunity to examine the structures of the FALS mutant CuZnSOD proteins and to look for features in these molecules that might alter the chemistry that occurs at the metal binding sites, perhaps by providing greater access to the catalytic site for unnatural substrates. No structures have yet been reported that show how FALS point mutations specifically affect the molecular architecture or activity of the mutant CuZnSODs relative to the wild-type protein. As experimental support grows for a gain of function for the FALS mutant CuZnSOD molecules (for a review, see Brown, 1995; Cudkowicz & Brown, 1996), three-dimensional structures of the mutant molecules should help in understanding the connection of FALS to CuZnSOD. As a first step in structural interpretation, we present the refined X-ray crystal structure of the human FALS mutant CuZnSOD G37R at 1.9 Å resolution.

Results

Quality of the atomic model

After refinement against X-ray data, the human G37R FALS mutant CuZnSOD model consists of 306 amino acid residues, 2,234 protein atoms, 177 water molecules, two copper ions, and two zinc ions. The subunits are N-acetylated in the yeast expression system as reported earlier (Hallewell et al., 1987; Wiedau-Pazos et al., 1996; our unpubl. mass spectrometry results). All atoms other than hydrogen are present in the final model. The crystallographic R-value for all data in the 10–1.9 Å shell (no σ cutoff) is 0.202 (R_{free} = 0.244). For the dimer, atomic displacement parameters average 27 ± 11 and 29 ± 13 Å^2 for backbone and all atoms, respectively.

The crystal has two subunits in the asymmetric unit, meaning that its two subunits—which we term subunit$_{intact}$ and subunit$_{broken}$—occupy different environments and have different properties. Atomic displacement parameters average 30 ± 10 Å^2 for the backbone atoms of subunit$_{intact}$, whereas those of subunit$_{broken}$ average 24 ± 11 Å^2. Overall RMSDs from ideality for bond lengths and angles are 0.01 Å and 1.7°, respectively. Ninety-nine percent of the amino acid residues have ϕ and ψ angles that fall in the allowed regions of a Ramachandran plot (Ramachandran & Sasiskharam, 1968).

Overall protein fold

As in other CuZnSOD molecules, G37R has an overall Greek key β-barrel topology. The refined structure shows essentially no gross deviations in backbone positions relative to the wild-type and thermostable mutant human CuZnSOD protein coordinates available in the Protein Data Bank (1spd, 1sos) (Parge et al., 1992; Deng et al., 1993). G37R and wild-type backbone atoms superimpose with an RMSD of 0.90 Å for 1,171 target pairs (0.32 Å for the thermostable mutant dimer formed by chains A and F, 1,154 target pairs). Figure 1B shows a superposition of backbones of G37R with the wild-type enzyme. Within the homodimer, the backbones of G37R subunit$_{intact}$ and subunit$_{broken}$ are very similar, superimposing with an RMSD of 0.21 Å for all backbone atoms. This superposition is shown in Figure 1C.

Glycine to arginine mutation sites

The glycine to arginine mutation does not cause significant rearrangement of the protein backbone in either subunit relative to wild type. Gly 37 has been reported as a conserved left-handed Gly in the wild-type protein (Deng et al., 1993). The G37R mutant also has left-handed conformation for Arg 37, with ϕ and ψ angles of 72.6° and 23.7° for subunit$_{intact}$ and 64.8° and 30.5° for subunit$_{broken}$. Atoms in the Arg 37 side chain in subunit$_{intact}$ have weak electron density and high atomic displacement parameters (~70 Å^2). Subunit$_{intact}$ Arg 37 is solvent exposed and not in close proximity to any symmetry-related molecules in the crystal lattice. Atoms in the side chain of Arg 37 in subunit$_{broken}$ have well-defined electron density. Subunit$_{broken}$ Arg 37 makes a weak electrostatic interaction with the side chain of Gln 153 (the C-terminal residue) of a symmetry-related molecule in the crystal lattice.

Copper and zinc binding sites

The copper ion environments in the two subunits differ as shown in Table 1. The copper center in subunit$_{intact}$ has a four-coordinate geometry with histidine ligands 46, 48, 63, and 120. The bridging imidazolate (His 63) coordinates both the copper and zinc ions at distances of 2.70 Å and 1.87 Å, respectively, and shows strong continuous electron density between it and the metal ions. The atomic displacement parameters for the copper and zinc ions in subunit$_{intact}$ are 40 Å^2 and 27 Å^2, respectively.

Subunit$_{broken}$ has a distorted trigonal planar geometry with the nearest water molecule residing 3.30 Å from the copper ion. His 63 coordinates only the zinc ion, at a distance of 1.81 Å. The electron density is continuous for its interaction with the zinc ion, but broken between itself and the copper ion. In this subunit, the copper atom is 2.95 Å from the NE2 atom of His 63. The atomic displacement parameters for the copper and zinc ions in subunit$_{broken}$ are 28 and 21 Å^2, respectively. Figure 2 shows the copper centers of both subunits superimposed on simulated annealing omit maps contoured at 1σ and ($F_o - F_c$) maps contoured at 3σ. The copper ion in subunit$_{broken}$ exhibits anisotropic vibration, as indicated by the difference density peaks above and below the position of the copper ion after refinement.

As a further verification of copper site asymmetry, we refined the G37R molecule using NCS restraints and constraints. Metal ions, ligand residues, and one residue N- and C-terminal to each ligand were restrained by a weight determined by monitoring R_{free}. All other atoms in the structure were constrained to obey the strict NCS operator. The resulting electron density maps confirmed the asymmetry we observed in $(2F_o - F_c)\alpha_c$, $(F_o - F_c)\alpha_c$, and annealed omit maps.

Electrostatic energy

The electrostatic potential at the copper ion in subunit$_{intact}$ and subunit$_{broken}$ was calculated via a Lekner (explicit, real-space) summation described in Materials and methods. These calculations suggest that the electrostatic potential at the copper ions in both subunit$_{intact}$ and subunit$_{broken}$ are essentially equivalent.

Table 1. *Comparison of Cu-ligand bond lengths and angles in yeast wild-type SOD (Ogihara et al., 1996), human FALS mutant G37R SOD (this study), and human wild-type SOD (1spd) (Deng et al., 1993)*[a]

	G37R Subunit$_{intact}$	G37R Subunit$_{broken}$	Yeast (broken)	WT Subunit A	WT Subunit B
Bond lengths (Å)					
Cu–His 46-ND1	2.15	2.08	2.06	2.05	2.15
Cu–His 48-NE2	2.28	2.11	2.06	2.13	2.13
Cu–His 63-NE2	2.70	2.95	3.16	2.09	2.15
Cu–His 120-NE2	2.09	2.00	2.10	2.08	2.02
Bond angles (degrees)					
His 46-ND1–Cu–His 48-NE2	140.2	143.9	138.5	139.6	125.0
His 46-ND1–Cu–His 63-NE2	76.7	[b]	[b]	89.6	59.5
His 46-ND1–Cu–His 120-NE2	107.9	94.1	102.9	78.2	95.4
His 48-NE2–Cu–His 63-NE2	96.3	[b]	[b]	95.9	83.0
His 48-NE2–Cu–His 120-NE2	104.7	115.3	118.5	91.8	98.4
His 63-NE2–Cu–His 120-NE2	134.4	[b]	[b]	167.5	147.7

[a] Yeast wild type has one unique subunit (monomer in asymmetric unit). G37R has two distinct subunits in the crystal ("intact" and "broken"). Human wild type has two distinct subunits in the crystal ("A" and "B"), but both have intact imidazolate bridges as judged by the Cu–His 63-NE2 bond lengths. G37R subunit$_{intact}$ has a longer than expected Cu–His 63-NE2 bond distance for an intact imidazolate bridge, but the electron density between these atoms is continuous (see text).

[b] The Cu–His 63 imidazolate bridge is broken in these structures.

Discussion

G37R mutation site and its proximity

The G37R mutation occurs in a region of the molecule where the three-dimensional architecture is considered critical for maintaining protein stability. An adjacent amino acid, Leu 38, has been termed the "plug" of one end of the β-barrel (Deng et al., 1993). Leu 38 fills a cavity formed by an array of apolar amino acids coming from different β-strands. These amino acids, Val 14, Ile 35, Leu 144, and the ring face of His 43 pack tightly around Leu 38. They are also themselves, with the exception of Ile 35, found as mutations in some FALS families [V14M (de Belleroche et al., 1996), L38V (Deng et al., 1993), H43R (Deng et al., 1993), L144F (Deng et al., 1993), and L144S (de Belleroche et al., 1996)]. The clustering of FALS mutations in this region of the β-barrel suggests that the wild-type packing arrangement of apolar residues is crucial for correct enzymatic function and protein stability (Deng et al., 1995).

There are structural reasons for the conservation of several glycine residues in the wild-type protein. The absence of side chains on left-handed glycine residues Gly 37, Gly 41, and Gly 93 seems necessary to support main-chain conformation and the packing interactions in the hydrophobic plug (Deng et al., 1995). The G37R mutation, while maintaining a left-handed conformation in the crystal structure, provides a bulky side chain that is free to sample many conformations and to interact with neighboring amino acid residues. This mobility, evidenced in the high atomic displacement parameters for Arg 37 in subunit$_{intact}$, coupled with close proximity to Leu 38, may diminish the tight packing interactions between Leu 38 and the other apolar plug residues described above. As mentioned previously, the G37R CuZnSOD is less stable than wild type (Borchelt et al., 1994).

The details of the 1.9 Å G37R structure, the first human CuZnSOD to be refined to a resolution finer than 2.4 Å, also suggest why Gly 93 is frequently observed as an FALS mutation site. Residues 90–93 form a tight β-hairpin turn separate from, but adjacent to the β-barrel packing interactions. Five mutations at this site, G93A (Deng et al., 1993), G93C (Borchelt et al., 1994), G93R (Elshafey et al., 1994), G93D (Esteban et al., 1994), and G93V (de Belleroche et al., 1996), have been identified. If residue 93 is not a glycine, the β-carbon of any inserted side chain will produce a steric clash with the carbonyl oxygen of Leu 38 and disrupt the backbone and possibly the packing of apolar residues in the β-barrel plug centered on residue 38. The G93C mutant, like G37R, shows a reduction in polypeptide stability (Borchelt et al., 1994). Figure 2C shows a superposition of the β-barrel plug and β-hairpin turn regions of the G37R subunit$_{intact}$ on the human wild-type protein 1spd (Deng et al., 1993)]. The figure illustrates the differences of the protein backbones and stabilizing side-chain interactions in this critical region of CuZnSOD.

The D90A FALS mutation is also part of the β-hairpin turn, which contains the site for the five known Gly 93 FALS mutations. Like G37R, there is no significant difference in enzyme activity between the D90A and wild-type CuZnSOD proteins (Sjalander et al., 1995). It has been postulated that the identity of residue 90 is not crucial for overall stability due to its solvent-exposed position (Sjalander et al., 1995).

The stability of the β-hairpin 90–93 may, however, be reduced by the loss of Asp 90. From our refined G37R crystal structure, it is observed that the Asp 90 side chain stabilizes this tight turn by reaching forward in sequence to accept a hydrogen bond from the amide nitrogen of residue 92. The distance between the donor amide nitrogen and the acceptor OD2 oxygen is 2.85 Å. Only one other hydrogen bond, that between the acceptor carbonyl oxygen of residue 90 and the proton donor amide nitrogen of residue 93 at a distance of 2.81 Å, stabilizes this turn. In the D90A mutant, the stabilizing effect of the hydrogen bond between the aspartic acid side chain and amide proton is lost. In the G37R structure, the atomic displacement parameters for main-chain atoms in this β-hairpin turn average 52 ± 5 Å^2 for subunit$_{intact}$, a large value, and 27 ± 3 Å^2 for subunit$_{broken}$. The loss of this hydrogen bond would allow this turn even more flexibility (see Fig. 2C).

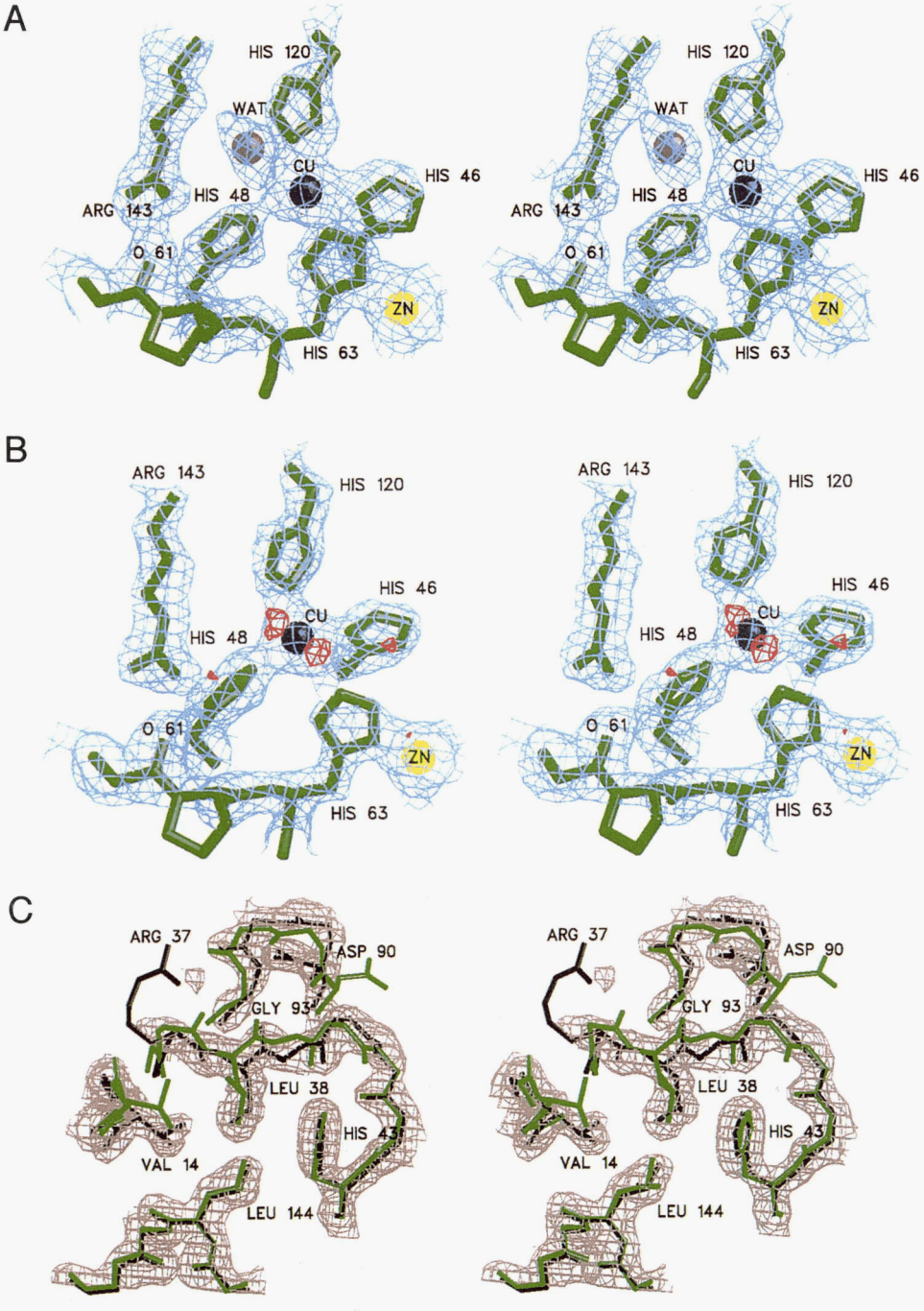

Fig. 2. Subunit$_{intact}$ and subunit$_{broken}$ copper binding sites superimposed on 1.9 Å electron density. Electron density (light blue) is a simulated annealing omit map of the form $(2F_o - F_c)\alpha_c$ contoured at 1σ, and calculated as described in Materials and methods. Copper ligands (His 46, His 48, His 63, His 120) and Arg 143 are shown as green tubes. The side chain of Arg 143 is believed to be important in the positioning of the superoxide for its interaction with the catalytic copper (Tainer et al., 1988; Getzoff et al., 1989, 1992). Copper and zinc ions are represented by blue and yellow spheres, respectively, and are shown in the same orientation as in Figure 1C. **A:** Subunit$_{intact}$. Note the continuous electron density between the copper atom and the bridging imidazolate, His 63. The water molecule, represented by a gray sphere, is ~2.9 Å from the copper ion. The side chain of Arg 143 makes a hydrogen bond with the carbonyl oxygen of Pro 61. **B:** Subunit$_{broken}$. Note that the continuous electron density between the copper atom and His 63 seen in A is absent. The copper is coordinated by a roughly trigonal-planar arrangement of histidine residues, suggestive of the Cu(I) oxidation state. The copper atom exhibits anisotropy represented by the red cages of electron density of the form $(F_o - F_c)\alpha_c$ contoured at 3σ. The carbonyl oxygen of Pro 61 accepts the HD1 proton from the ND1 atom of His 48. **C:** β-Barrel "plug" (Deng et al., 1993) and β-hairpin turn regions of G37R subunit$_{intact}$ (black) and wild-type subunit "A" (green) CuZnSOD superimposed on each other and on 1.9 Å G37R electron density. The electron density (gray) is of the form $(2F_o - F_c)\alpha_c$ contoured at 1σ. The view is approximately the same as in Figure 1C. Only side chains found to be mutated in FALS are shown. The Arg 37 side chain in subunit$_{intact}$ has high thermal parameters. Val 14, His 43, and Leu 144 form a cavity filled by Leu 38. The alpha carbon of Gly 93 is immediately above the Gly 93 label. Any side-chain insertion at position 93 would cause steric clash with the carbonyl oxygen of Leu 38 (see text). The Asp 90 side chain in G37R accepts a hydrogen bond from the amide nitrogen of residue 92, stabilizing the β-hairpin turn (see text).

G37R versus wild type

As stated above, human G37R CuZnSOD exhibits few distortions in backbone structure relative to the wild-type enzyme (RMSD = 0.90 Å for backbone atoms). There are, however, significant differences between G37R and wild type in the geometries of the copper-binding residues (Table 1 and below). The model of the wild-type enzyme (1spd) shows the imidazolate bridge as intact in both subunits, suggesting that the copper is in its Cu(II) state (Deng et al., 1993). This wild-type model agrees with previous crystallographic models of bovine, spinach, yeast, and frog CuZnSODs (Tainer et al., 1982, 1983; Kitagawa et al., 1991; Djinovic et al., 1992; Djinovic-Carugo et al., 1994).

In contrast, G37R has the imidazolate bridge intact in one subunit and broken in the other. One possible explanation for this observation would be the existence of differential oxidation states of the copper ion in the same molecule. The only previous CuZnSOD X-ray structure observed with a broken imidazolate bridge is yeast wild-type CuZnSOD, which was confirmed to be in the Cu(I) state by EPR (Ogihara et al., 1996).

Copper site asymmetry in G37R

What causes the copper ions to have different coordination environments in $subunit_{intact}$ and $subunit_{broken}$ in G37R CuZnSOD? It is possible the G37R molecules in solution are asymmetric and then pack into the crystal lattice with a uniform orientation. Although the G37R CuZnSOD structure presented in this crystallographic study is the first to show significant differences between the two active sites, a recent 100-ps molecular dynamics simulation (MD) on the whole bovine dimer suggested the occurrence of two different conformational substates for the two active sites in the monomers (Falconi et al., 1996). A subsequent MD study on the bovine enzyme indicated an instantaneous asymmetric dynamical behavior of the two monomers. The largest displacements were confined to the region of the active site loops, and the presence of correlated motions suggested the occurrence of a mechanical coupling between the two subunits (Chillemi et al., 1997). Conceivably, this mechanical coupling could be exaggerated in the G37R CuZnSOD molecule, allowing active site asymmetry to be observed in the crystal.

Alternatively, molecules with symmetrical subunits could pack into the crystal lattice, followed by the generation of the copper site asymmetry. This asymmetry could arise from different crystal packing forces or from different electrostatic potentials at the copper ions (which have different environments) in the crystal. Figure 2B shows that the refined backbone positions of $subunit_{intact}$ and $subunit_{broken}$ are very similar, superimposing with an RMSD of 0.21 Å for all backbone atoms. This similarity gives no suggestion that lattice forces cause the apparent copper site asymmetry.

Calculation of the electrostatic potential at the copper ions in $subunit_{intact}$ and $subunit_{broken}$ via an Lekner summation reveals no significant difference. Thus, there is no reason to believe that different electrostatic potentials at the two copper sites are responsible for the observed copper site asymmetry.

The electron density clearly shows a bond between the copper ion and the NE2 atom of His 63 in $subunit_{intact}$ and the lack of a bond between these atoms in $subunit_{broken}$ (Fig. 2A,B). If one assumes this difference is due to redox asymmetry, the details of the ligand geometry suggest a minor mixture of oxidation states in $subunit_{intact}$ and $subunit_{broken}$. The bond angles and lengths for the copper and its ligands in $subunit_{intact}$ are nonstandard for a putative pure Cu(II) redox state. That is, the copper and zinc ions do not both lie in the plane of the imidazolate bridge (His 63) in the refined structure of $subunit_{intact}$, and the bond length from the copper ion to the NE2 atom of His 63 is longer (~2.7 Å) than expected (~2.1 Å) for a pure Cu(II) oxidation state. If the G37R molecules in solution are asymmetric (each molecule has an intact and broken imidazolate bridge) prior to crystallization and some of these asymmetric molecules "flip" upon crystallization, we would observe an averaged structure at each copper binding site; then the "bridge-intact" site would then have some "bridge-broken" character and vice versa. That is, it is possible that the ratio of imidazolate bridge-broken to bridge-intact subunits in the crystal is not 50:50. The bridge-broken species may predominate, and the observed bridge-intact electron density and long copper-His 63 bond length in $subunit_{intact}$ could arise from such a mixture. It should be stressed that we imposed no stereochemical constraints on metal–ligand bond distances and angles during the course of refinement. It is also possible that the asymmetry in subunit atomic displacement parameters could play a role in the generation of the copper site asymmetry (see below).

Atomic displacement parameter asymmetry in G37R

In addition to copper ligand asymmetry between the two subunits in G37R CuZnSOD, there is marked asymmetry in their atomic displacement parameters. Atoms in $subunit_{intact}$ have higher atomic displacement parameters than do atoms in $subunit_{broken}$. Backbone atoms average 30 ± 10 $Å^2$ in $subunit_{intact}$ and 24 ± 11 $Å^2$ in $subunit_{broken}$. Even more striking is the difference between atomic displacement parameters for the copper atoms in $subunit_{intact}$ (40 $Å^2$) and $subunit_{broken}$ (28 $Å^2$). An atomic displacement parameter of 40 $Å^2$ might suggest partial occupancy of copper in $subunit_{intact}$. If this is the case, the apoCu forms of the molecule, which might indeed be looser, could contribute to the overall atomic displacement parameter asymmetry observed in the two subunits. Figure 3 shows the G37R homodimer backbone color coded by main-chain atomic displacement parameter values. Residues 133–144 in $subunit_{intact}$ have considerably higher atomic displacement parameters (ranging from approximately 30 to 50 $Å^2$) than does the same range of residues in $subunit_{broken}$ (ranging from approximately 14 to 29 $Å^2$). These residues form one half of what could be termed the "rim" of the active site channel leading to the copper ion, and include Glu 132, Glu 133, Lys 136, Thr 137, and Arg 143, residues postulated as critical for the electrostatic guidance of substrate into the active site (Tainer et al., 1988; Getzoff et al., 1989, 1992). In particular, the mobility of residues forming the sides of the active site channel, Arg 143 and Thr 137, can increase or decrease the availability of the copper ion for interaction with substrate. Atomic displacement parameters for backbone atoms for Thr 137 and Arg 143 average 32 ± 0.9 $Å^2$ and 33 ± 0.9 $Å^2$, respectively, in $subunit_{intact}$ and 23 ± 0.4 $Å^2$ and 16 ± 1 $Å^2$, respectively, in $subunit_{broken}$. These "rim" residues in the human wild-type protein (Deng et al., 1993) exhibit neither the atomic displacement parameter asymmetry nor the relative high atomic displacements observed for these residues in G37R $subunit_{intact}$.

The greater values observed for main-chain atomic displacement parameters for $subunit_{intact}$ compared with $subunit_{broken}$ may be due to tighter crystal packing around $subunit_{broken}$. $Subunit_{intact}$ is held in the crystal lattice by two main contact regions with neighboring molecules, whereas $subunit_{broken}$ is held in the lattice

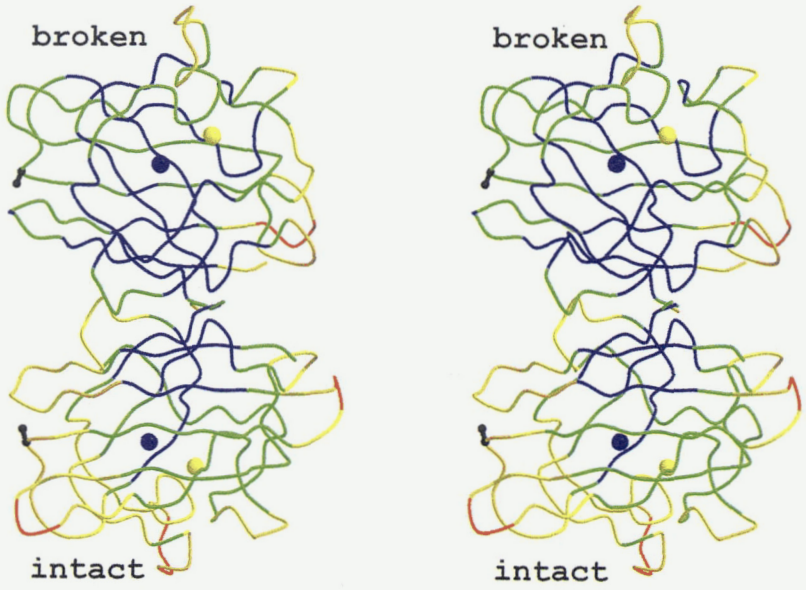

Fig. 3. Color-coded main-chain atomic displacement parameters. This view is the same as in Figure 1A and B. $Subunit_{intact}$ is on the bottom and $subunit_{broken}$ is on the top. Main-chain atoms are color coded by the values of their atomic displacement parameters as follows: 0–20 Å^2 (blue); 20–30 Å^2 (green); 30–40 Å^2 (yellow); 40–50 Å^2 (orange); >50 Å^2 (red). $Subunit_{intact}$ has a large amount of yellow color (large atomic displacements) on the solvent side of the catalytically active copper center, whereas $subunit_{broken}$ has none. The copper and zinc atoms are represented by blue and yellow spheres, respectively, but are not color coded for their atomic displacement parameters. The G37R mutation position is shown as a black ball-and-stick β-carbon.

by four neighbors. Neither subunit, however, makes a crystal contact utilizing the "rim" residues 133–144 that are important in the putative electrostatic guidance of substrate and in the creation of the narrowing channel used in substrate discrimination.

If the higher atomic displacement parameters for $subunit_{intact}$ are due to fewer lattice interactions than are seen for $subunit_{broken}$, it is likely that, in solution, away from intermolecular constraints, both monomers of the dimer are flexible. The G37R molecule, flexible in solution, may have a predominantly imidazolate bridge-intact conformation. When one subunit of the molecule is constrained in the crystal lattice, as seen in the G37R case, it may adopt the bridge-broken conformation. In support of this hypothesis, yeast CuZnSOD, which packs in a highly constrained crystal lattice (R32), exhibits a predominantly Cu(I) oxidation state (Ogihara et al., 1996). Main-chain (20 ± 8 Å^2) and copper ion (26 Å^2) atomic displacement parameters for the yeast CuZnSOD, which has a monomer in the asymmetric unit, exhibit values similar to those for $subunit_{broken}$ in G37R (24 ± 11 Å^2 and 28 Å^2) (Ogihara et al., 1996). Thus, perhaps there is a link between the rigidity of the structure and a predisposition to a given copper ion liganding configuration. Solution experiments are needed to examine the apparent redox asymmetry of G37R CuZnSOD in more detail.

G37R and its connection to FALS

Analysis of the refined structure of G37R CuZnSOD and its comparison to wild type does not produce an unambiguous hypothesis as to how the mutant protein might cause FALS, but it does offer hints. The refined G37R structure is unusual in that it exhibits asymmetry in both copper site coordination and atomic displacement parameters. The copper site asymmetry has not been observed in any other CuZnSOD structure. As explained above, however, it is not clear if this asymmetry is caused by crystallization or is a property of the mutant molecule itself. If it is the molecule itself, then the existence of asymmetry might be a sign of CuZnSOD malfunction.

Even if the asymmetry is caused by crystallization, our results imply that the G37R molecule is flexible. This flexibility is especially evident in $subunit_{intact}$, the less-constrained subunit in the crystal, where the main-chain and the copper ion itself have unusually high atomic displacement parameters. Because G37R CuZnSOD retains full specific activity, the key to its role in FALS onset may be this flexibility rather than the copper site geometry. Copper ions and copper coordination complexes are frequently quite toxic, presumably due to their ability to promote adverse oxidation reactions. This mode of toxicity is repressed in normal copper proteins such as CuZnSOD, presumably by limiting access of substrates to the copper site and modulating the reactivity of the copper ion by adjusting its coordination environment. A loosening of the protein structure of CuZnSOD in FALS mutants may de-repress this inherent toxicity of the copper center, converting the enzyme-bound coppper ion into a "wolf in sheep's clothing." To answer these questions, more structures of FALS mutant CuZnSODs are needed for analysis.

Materials and methods

Preparation of human wild-type and mutant CuZnSOD molecules has been described previously (Wiedau-Pazos et al., 1996). In this case, a DNA fragment encoding the human G37R CuZnSOD mutant protein was generated by PCR mutagenesis of the human wild-type SOD gene, and the full sequence was determined for verification of correctness. The mutant gene was cloned under the control of the yeast CuZnSOD promoter in the yeast shuttle vector

YEP351, and transformed into yeast strain EG118, which has its endogenous CuZnSOD gene deleted (Rabizadeh et al., 1995). Cultures of 10 L were grown in aerated YEPD medium (1% yeast extract, 2% peptone, and 2% dextrose) for 36 h. Cells were harvested by centrifugation, resuspended in a small volume, and lysed with an equal volume of 0.5-mm glass beads in a blender. Protein purification was as described (Lu et al., 1993), with the addition of a final Sephadex G75 (Pharmacia) chromatography step. The purified protein (~50 mg) was homogeneous as indicated by SDS-PAGE. Human CuZnSOD expressed in yeast is acetylated normally at the NH_2-terminus (Hallewell et al., 1987; our unpubl. results). Copper and zinc ions were removed and the apoenzymes were recombined with metal by the gradual addition of $CuSO_4$ and $ZnSO_4$ (Nishida et al., 1994).

Crystals of human G37R CuZnSOD were obtained by the hanging drop vapor diffusion method and contain one homodimer per asymmetric unit. High-resolution crystallographic data were collected to 1.9 Å resolution on a rotating anode X-ray generator equipped with an imaging plate detector. Table 2 summarizes parameters and statistics of crystallization and data collection. The 2.5 Å model of human wild-type CuZnSOD [1spd (Deng et al., 1993)] was employed as the search model in cross rotation and translation functions. Rotation and translation functions were performed with the AMORE program package (Navaza, 1994) using 100–4.0 Å data and varying radii of integration. The rotation searches gave an unambiguous solution after Patterson correlation refinement. Translation searches revealed the correct enantiomer to be space group $P4_1$. Rigid-body refinement in XPLOR (Brünger, 1988) gave an R-value of 44.3% (R_{free} = 47.5%) using 10–3.0 Å data.

Table 2. *Crystallographic data for G37R CuZnSOD*[a]

Space group	$P4_1$
Unit cell dimensions (Å)	$a = b = 67.2$, $c = 83.8$
Asymmetric unit	1 G37R CuZnSOD homodimer
Temperature (°C)	20
Wavelength (Å)	1.54
Crystal-to-plate distance (mm)	120
Oscillation range (°)	1.5
No. observations	101,819
No. unique reflections	29,129
Completeness (%)[b]	99.1 (99.6[c])
Resolution limit (Å)	1.90
R_{sym} (%)[d]	6.5 (38.3[c])

[a]Five microliters of protein solution at ~20 mg/mL in 10 mM acetate buffer, pH 5.5, was mixed with 5 μL of reservoir solution (solution 47, Crystal Screen I, Hampton Research) containing 100 mM Na acetate, pH 4.6, 2.0 M ammonium sulfate, and allowed to equilibrate at room temperature. Large bipyramids (0.35 × 0.35 × 0.35 mm) grew within one month in space group $P4_1$ with unit cell parameters $a = b = 67.2$ Å, $c = 83.8$ Å. Three-dimensional diffraction data were collected to 1.9 Å resolution using a Rigaku RAXIS IV imaging plate detector. The X-ray source was a Rigaku RU-200 generator with focusing mirrors running at 50 kV, 100 mA. Crystals were rotated about ϕ, and oscillation images were collected every 1.5°. The data were reduced using the program DENZO (Otwinowski, 1993) to 1.9 Å (99.1% complete) with an R_{sym} (on I) of 6.5%. Data in the highest resolution shell (1.97–1.90 Å) were 99.6% complete.

[b]Of all reflections to 1.9 Å.

[c]These numbers denote completeness in the highest-resolution shells (1.97–1.90 Å).

[d]R_{sym} = conventional discrepancy R-factor for scaling symmetry-related intensities.

Model building was undertaken using all data (no σ cutoff) during six rounds of crystallographic refinement in XPLOR. A "round" of refinement is defined as sequential utilization of positional, simulated annealing, and isotropic temperature factor refinement routines, followed by visual inspection of electron density maps coupled with manual model rebuilding (when necessary), using the molecular graphics FRODO (Jones, 1978). No stereochemical constraints were imposed on the coordination geometries of the copper and zinc ions during refinement. Model atom positions were verified by the examination of conventional and simulated annealing omit maps (Hodel et al., 1992). One-hundred seventy-seven water molecules were incorporated into the model during the refinement process, with a final R-value of 0.202 (R_{free} = 0.244) for all 28,975 reflections in the 10–1.9 Å shell.

Structural alignment of backbone atoms of the G37R monomers $subunit_{intact}$ and $subunit_{broken}$ onto each other and the G37R dimer onto human wild-type dimer [1spd (Deng et al., 1993)] and the human thermostable mutant [1sos (Parge et al., 1992)] was accomplished using a modified version of the program ALIGN (Satow et al., 1986). Simulated-annealing omit maps (Hodel et al., 1992) around metal atoms were calculated by omitting a 6 Å radius sphere around both the copper and zinc atoms and heating to 2500 K during the simulated-annealing protocol. NCS refinement was performed by applying strict NCS constraints to all atoms other than the metal ions, their ligands, and one residue N- and C-terminal to the ligand residues. Varying NCS-restraint weights were then applied to these nonconstrained atoms while monitoring R_{free}. The model corresponding to the best weight (lowest R_{free}) was used to calculate electron density maps. Electrostatic energy was calculated using the Lekner summation algorithm written by Niels Grønbech-Jensen (Grønbech-Jensen, 1998). The analysis covers explicit expressions for energy constants and self-energies of charged particles in periodic lattices (Grønbech-Jensen, 1998). Figure 2 was generated with the molecular graphics program SETOR (Evans, 1993). Figures 1 and 3 were created with the molecular graphics program MOLSCRIPT (Kraulis, 1991) and rendered with Raster3D version 2.1 (Bacon & Anderson, 1988; Merrit & Murphy, 1994). Atomic coordinates and diffraction data have been deposited in the Brookhaven Protein Data Bank with codes 1azv and r1azvsf, respectively.

Acknowledgments

Discussions with D. Cascio, N. Ogihara, T. Lyons, J. Goto, J. Roe, and D. Bredesen are gratefully acknowledged. N. Grønbech-Jensen developed the Lekner algorithm used in this study. This research was supported by grants from the Amyotrophic Lateral Sclerosis Association (ALSA) (award #012591, D.E.), NIH (GM31299, D.E.), (GM28222, J.S.V.), and the DOE (DE-FC03-87ER60615).

References

Aoki M, Ogasawara M, Matsubara Y, Narisawa K, Nakamura S, Itoyama Y, Abe K. 1994. Familial amyotrophic lateral sclerosis (ALS) in Japan associated with H46R mutation in Cu/Zn superoxide dismutase gene: A possible new subtype of familial ALS. *J Neurol Sci 126*:77–83.

Bacon DJ, Anderson WF. 1988. A fast algorithm for rendering space-filling molecule pictures. [Abstract of article presented at the Seventh Annual Meeting of the Molecular Graphics Society] *J Mol Graph* 6:219–220.

Banci L, Bertini I, Bruni B, Carloni P, Luchinat C, Mangani S, Orioli PL, Piccioli M, Rypniewski WR, Wilson KS. 1994. X-ray, NMR and molecular dynamics studies on reduced bovine superoxide dismutase: Implications for the mechanism. *Biochem Biophys Res Commun 202*:1088–1095.

Bannister JV, Bannister WH, Rotilio G. 1987. Aspects of the structure, function, and applications of superoxide dismutase. *CRC Crit Rev Biochem 22*:111–180.

Beckman JS, Carson M, Smith CD, Koppenoll WH. 1993. ALS, SOD and peroxynitrite. *Nature 364*:584 (Letter).

Beckman JS, Ischiropoulos H, Zhu L, van der Woerd M, Smith C, Chen J, Harrison J, Martin JC, Tsai M. 1992. Kinetics of superoxide dismutase- and iron-catalyzed nitration of phenolics by peroxynitrite. *Arch Biochem Biophys 298*:438–445.

Bertini I, Banci L, Piccioli M. 1990. Spectroscopic studies on Cu_2Zn_2SOD: A continuous advancement in investigation tools. *Coord Chem Rev 100*:67–103.

Bertini I, Luchinat C, Monnanni R. 1985. Evidence of the breaking of the copper-imidazolate bridge in copper/cobalt-substituted superoxide dismutase upon reduction of the copper(II) center. *J Am Chem Soc 107*:2178–2179.

Blackburn NJ, Hasnain SS, Binsted N, Diakun GP, Garner CD, Knowles PF. 1984. An extended-X-ray-absorption-fine-structure study of bovine erythrocyte superoxide dismutase in aqueous solution. Direct evidence for three-coordinate Cu(I) in reduced enzyme. *Biochem J 219*:985–990.

Borchelt DR, Lee MK, Slunt HS, Guarnieri M, Xu ZS, Wong PC, Brown RH, Price DL, Sisodia SS, Cleveland DW. 1994. Superoxide dismutase 1 with mutations linked to familial amyotrophic lateral sclerosis possesses significant activity. *Proc Natl Acad Sci USA 91*:8292–8296.

Brown RH. 1995. Superoxide dismutase in familial amyotrophic lateral sclerosis: Models for gain of function. *Curr Opin Neurobiol 5*:841–846.

Bruijn LI, Beal MF, Becher MW, Schulz JB, Wong PC, Price DL, Cleveland DW. 1997. Elevated free nitrotyrosine levels, but not protein-bound nitrotyrosine or hydroxyl radicals, throughout amyotrophic lateral sclerosis (ALS)-like disease implicate tyrosine nitration as an aberrant in vivo property of one familial ALS-linked superoxide dismutase 1 mutant. *Proc Natl Acad Sci USA 94*:7606–7611.

Brünger AT. 1988. Crystallographic refinement by simulated annealing. In: Issacs NW, Taylor MR, eds. *Crystallographic computing 4: Techniques and new technologies*. Oxford: Clarendon Press. pp 126–140.

Cabelli DE, Allen D, Bielski BH, Holcman J. 1989. The interaction between Cu(I) superoxide dismutase and hydrogen peroxide. *J Biol Chem 264*:9967–9971.

Carri MT, Battistoni A, Polizio F, Desideri A, Rotilio G. 1994. Impaired copper binding by the H46R mutant of human Cu,Zn superoxide dismutase, involved in amyotrophic lateral sclerosis. *FEBS Lett 356*:314–316.

Chillemi G, Falconi M, Amadei A, Zimatore G, Desideri A, Di Nola A. 1997. The essential dynamics of Cu,Zn superoxide dismutase: Suggestion of intersubunit communication. *Biophys J 73*:1007–1018.

Cleveland DW, Bruijn LI, Wong PC, Marszalek JR, Vechio JD, Lee MK, Xu XS, Borchelt DR, Sisodia SS, Price DL. 1996. Mechanisms of selective motor neuron death in transgenic mouse models of motor neuron disease. *Neurology 47*:54–62.

Cudkowicz ME, Brown RH. 1996. An update on superoxide dismutase 1 in familial amyotrophic lateral sclerosis. *J Neurol Sci 139*:10–15.

Dal Canto MC, Gurney ME. 1995. Neuropathological changes in two lines of mice carrying a transgene for mutant human Cu,Zn SOD, and in mice overexpressing wild type human SOD: A model of familial amyotrophic lateral sclerosis (FALS). *Brain Res 676*:25–40.

de Belleroche J, Orrell RW, Virgo L. 1996. Amyotrophic lateral sclerosis: Recent advances in understanding disease mechanisms. *J Neuropath Exp Neurol 55*:747–757.

Deng HX, Hentati A, Tainer JA, Iqbal Z, Cayabyab A, Hung WY, Getzoff ED, Hu P, Herzfeldt B, Roos RP, Warner C, Deng G, Soriano E, Smyth C, Parge HE, Ahmed A, Roses AD, Hallewell RA, Pericak-Vance MA, Siddique T. 1993. Amyotrophic lateral sclerosis and structural defects in Cu,Zn superoxide dismutase. *Science 261*:1047–1051.

Deng HX, Tainer JA, Mitsumoto H, Ohnishi A, He X, Hung WY, Zhao Y, Juneja T, Hentati A, Siddique T. 1995. Two novel SOD1 mutations in patients with familial amyotrophic lateral sclerosis. *Hum Molec Genet 4*:1113–1116.

Djinovic K, Gatti G, Coda A, Antolini L, Pelosi G, Desideri A, Falconi M, Marmocchi F, Rotilio G, Bolognesi M. 1992. Crystal structure of yeast Cu,Zn superoxide dismutase. Crystallographic refinement at 2.5 Å resolution. *J Mol Biol 225*:791–809.

Djinovic-Carugo K, Battistoni A, Carri MT, Polticelli F, Desideri A, Rotilio G, Coda A, Bolognesi M. 1994. Crystal structure of the cyanide-inhibited *Xenopus laevis* Cu,Zn superoxide dismutase at 98 K. *FEBS Lett 349*:93–98.

Elshafey A, Lanyon WG, Connor JM. 1994. Identification of a new missense point mutation in exon 4 of the Cu/Zn superoxide dismutase (SOD-1) gene in a family with amyotrophic lateral sclerosis. *Hum Molec Genet 3*:363–364.

Enayat ZE, Orrell RW, Claus A, Ludolph A, Bachus R, Brockmüller J, Ray-Chaudhuri K, Radunovic A, Shaw C, Wilkinson J, King A, Swash M, Leigh PN, de Belleroche J, Powell J. 1995. Two novel mutations in the gene for copper zinc superoxide dismutase in UK families with amyotrophic lateral sclerosis. *Hum Molec Genet 4*:1239–1240.

Epstein CJ, Avraham KB, Lovett M, Smith S, Elroy-Stein O, Rotman G, Bry C, Groner Y. 1987. Transgenic mice with increased Cu/Zn superoxide dismutase activity: Animal model of dosage effects in Down syndrome. *Proc Natl Acad Sci USA 84*:8044–8048.

Esteban J, Rosen DR, Bowling AC, Sapp P, McKenna-Yasek D, O'Regan JP, Beal MF, Horvitz HR, Brown RH. 1994. Identification of two novel mutations and a new polymorphism in the gene for Cu/Zn superoxide dismutase in patients with amyotrophic lateral sclerosis. *Hum Molec Genet 3*:997–998.

Evans SV. 1993. SETOR: Hardware lighted three-dimensional solid model representations of macromolecules. *J Mol Graph 11*:134–138.

Falconi M, Gallimbeni R, Paci E. 1996. Dimer asymmetry in superoxide dismutase studied by molecular dynamics simulation. *J Comp-Aided Mol Design 10*:490–498.

Fielden EM, Roberts PB, Bray RC, Lowe DJ, Mautner GN, Rotilio G, Calabrese L. 1974. Mechanism of action of superoxide dismutase from pulse radiolysis and electron paramagnetic resonance: Evidence that only half the active sites function in catalysis. *Biochem J 139*:49–60.

Fridovich I. 1989. Superoxide dismutases. An adaption to a paramagnetic gas. *J Biol Chem 264*:7761–7764.

Getzoff ED, Cabelli DE, Fisher CL, Parge HE, Viezzoli MS, Banci L, Hallewell RA. 1992. Faster superoxide dismutase mutants designed by enhancing electrostatic guidance. *Nature 358*:347–351.

Getzoff ED, Tainer JA, Stempien MM, Bell GI, Hallewell RA. 1989. Evolution of Cu,Zn superoxide dismutase and the Greek key β-barrel structural motif. *Proteins Struct Funct Genet 5*:322–336.

Grønbech-Jensen N. 1997. Lekner summation of long range interactions in periodic systems. *J Mod Phys 8*:1287–1298.

Gurney ME, Pu H, Chiu AY, Dal Canto MC, Polchow CY, Alexander DD, Caliendo J, Hentati A, Kwon YW, Deng HX, Chen W, Zhai P, Sufit RL, Siddique T. 1994. Motor neuron degeneration in mice that express a human Cu/Zn superoxide dismutase mutation. *Science 264*:1772–1775.

Hallewell RA, Mills R, Tekamp-Olson P, Blacher R, Rosenberg S, Otting F, Masiarz FR, Scandella CJ. 1987. Amino terminal acetylation of authentic human Cu,Zn superoxide dismutase produced in yeast. *Biotechnology 5*:363–366.

Haverkamp LJ, Appel V, Appel SH. 1995. Natural history of aymotrophic lateral sclerosis in a database population. Validation of a scoring system and a model for survival prediction. *Brain 118*:707–719.

Hodel A, Kim SH, Brünger AT. 1992. Model bias in macromolecular crystal structures. *Acta Crystallogr A 48*:851–858.

Hodgson EK, Fridovich I. 1975. The interaction of bovine erythrocyte superoxide dismutase with hydrogen peroxide: Chemiluminescence and peroxidation. *Biochemistry 14*:5299–52303.

Ischiropoulos H, Zhu L, Chen J, Tsai M, Martin JC, Smith CD, Beckman JS. 1992. Peroxynitrite-mediated tyrosine nitration catalyzed by superoxide dismutase. *Arch Biochem Biophys 298*:431–437.

Jones TA. 1978. A graphics model building and refinement system for macromolecules. *J Appl Crystallogr 11*:268–272.

Juneja T, Pericak-Vance MA, Laing NG, Dave S, Siddique T. 1997. Prognosis in familial amyotrophic lateral sclerosis: Progression and surivial in patients with glu100gly and ala4val mutations in Cu,Zn superoxide dismutase. *Neurology 48*:55–57.

Kitagawa Y, Tanaka N, Hata Y, Kusonoki M, Lee GP, Katsube Y, Asada K, Aibara S, Morita YJ. 1991. Three-dimensional structure of Cu,Zn superoxide dismutase from spinach at 2.0 Å resolution. *J Biochem (Tokyo) 109*:477–485.

Klug-Roth D, Fridovich I, Rabini J. 1973. Pulse radiolytic investigations of superoxide catalyzed disproportionation: Mechanism for bovine superoxide dismutase. *J Am Chem Soc 95*:2786–2790.

Kraulis PJ. 1991. MOLSCRIPT: A program to produce both detailed and schematic plots of protein structures. *J Appl Crystallogr 24*:946–950.

Levanon D, Lieman-Hurwitz J, Dafni N, Wigderson M, Sherman L, Bernstein Y, Laver-Rudich Z, Danciger E, Stein O, Groner Y. 1985. Architecture and anatomy of the chromosomal locus in human chromosome 21 encoding the Cu/Zn superoxide dismutase. *EMBO J 4*:77–84.

Lu Y, Gralla EB, Valentine JS. 1993. Metalloprotein redesign: Characterization of copper-cysteinate proteins derived from yeast copper-zinc superoxide dismutase. *J Am Chem Soc 115*:5907.

Merrit EA, Murphy MEP. 1994. Raster3D Version 2.0—A program for photorealistic molecular graphics. *Acta Crystallogr D 50*:869–873.

Murphy LM, Strange RW, Hasnain SS. 1997. A critical assessment of the evidence from XAFS and crystallography for the breakage of the imidazolate bridge during catalysis in CuZn superoxide dismutase. *Structure 5*:371–379.

Navaza J. 1994. AMORE—An automated package for molecular replacement. *Acta Crystallogr D 50*:157–163.

Nishida CR, Gralla EB, Valentine JS. 1994. Characterization of three yeast copper-zinc superoxide dismutase mutants analogous to those coded for in familial amyotrophic lateral sclerosis. *Proc Natl Acad Sci USA 91*:9906–9910.

Ogihara NL, Parge HE, Hart PJ, Weiss MS, Goto JJ, Crane BR, Tsang J, Slater K, Roe JA, Valentine JS, Eisbenberg D, Tainer JA. 1996. Unusual trigonal-planar copper configuration revealed in the atomic structure of yeast copper-zinc superoxide dismutase. *Biochemistry 35*:2316–2321.

Otwinowski Z. 1993. Oscillation data reduction program. In: *Proceedings of the CCP4 study weekend: Data collection and processing*. Compiled by Sawyer L, Issacs N, Bailey S. SERC Laboratory, England. pp 56–62.

Pardo CA, Xu Z, Borchelt DR, Price DL, Sisodia SS, Cleveland DW. 1995. Superoxide dismutase is an abundant component in cell bodies, dendrites, and axons of motor neurons and in a subset of other neurons. *Proc Natl Acad Sci USA 92*:954–958.

Parge HE, Hallewell RA, Tainer JA. 1992. Atomic structures of wild-type and thermostable mutant recombinant human Cu,Zn superoxide dismutase. *Proc Natl Acad Sci USA 89*:6109–6113.

Rabizadeh S, Gralla EB, Borchelt DR, Gwinn R, Valentine JS, Sisodia SS, Wong P, Lee M, Hahn H, Bredesen DE. 1995. Mutations associated with amyotrophic lateral sclerosis convert superoxide dismutase from an anti-apoptotic gene to a proapoptotic gene: Studies in yeast and neural cells. *Proc Natl Acad Sci USA 92*:3024–3028.

Ramachandran GN, Sasiskharam V. 1968. Conformation of polypeptides and proteins. *Adv Protein Chem 23*:283–437.

Reaume AG, Elliott JL, Hoffman EK, Kowall NW, Ferrante RJ, Siwek DF, Wilcox HM, Flood DG, Beal MF, Brown RH, Scott RW, Snider WD. 1996. Motor neurons in Cu/Zn superoxide dismutase-deficient mice develop normally but exhibit enhanced cell death after axonal injury. *Nature Genet 13*:43–47.

Ripps ME, Huntley GW, Hof PR, Morrison JH, Gordon JW. 1995. Transgenic mice expressing an altered murine superoxide dismutase gene provide an animal model of amyotrophic lateral sclerosis. *Proc Natl Acad Sci USA 92*:689–693.

Rosen DR, Siddique T, Patterson D, Figlewicz DA, Sapp P, Hentati A, Donaldson D, Goto J, O'Regan JP, Deng HX, Rahmani Z, Krizus A, McKenna-Yasek D, Cayabyab A, Gaston SM, Berger R, Tanzi RE, Halperin JJ, Herzfeldt B, Van den Bergh R, Hung WY, Bird T, Deng G, Mulder DW, Smyth C, Laing NG, Soriano E, Pericak-Vance MA, Haines J, Rouleau GA, Gusella JS, Horvitz HR, Brown RH. 1993. Mutations in Cu/Zn superoxide dismutase gene are associated with familial amyotrophic lateral sclerosis. *Nature 362*:59–62.

Rotilio G, Bray RC, Felden EM. 1972. A pulse radiolysis study of superoxide dismutase. *Biochim Biophys Acta 268*:605–609.

Rotilio G, Morpurgo L, Giovagnoli C, Calabrese L, Mondovi B. 1971. Studies of metal sites of copper proteins: Symmetry of copper in bovine superoxide dismutase and its functional significance. *Biochemistry 11*:2187–2192.

Rypniewski WR, Mangani S, Bruni B, Orioli PL, Casati M, Wilson KS. 1995. Crystal structure of reduced bovine erythrocyte superoxide dismutase at 1.9 Å resolution. *J Mol Biol 251*:282–296.

Satow Y, Cohen GH, Padlan EA, Davies DR. 1986. Phosphocholine binding immunoglobulin Fab McPC603. An X-ray diffraction study at 2.7 Å. *J Mol Biol 190*:593–604.

Siddique T, Deng HX. 1996. Genetics of amyotrophic lateral sclerosis. *Hum Molec Genet 5*:1465–1470.

Sjalander A, Beckman G, Deng HX, Iqbal Z, Tainer JA, Siddique T. 1995. The D90A mutation results in a polymorphism of Cu,Zn superoxide dismutase that is prevalent in northern Sweden and Finland. *Hum Molec Genet 4*:105–1108.

Tainer JA, Getzoff ED, Beem KM, Richardson JS, Richardson DC. 1982. Determination and analysis of the 2 Å structure of copper, zinc superoxide dismutase. *J Mol Biol 160*:181–217.

Tainer JA, Getzoff ED, Richardson JS, Richardson DC. 1983. Structure and mechanism of copper, zinc superoxide dismutase. *Nature 306*:284–287.

Tainer JA, Hallewell RA, Roberts VR, Parge HE, Getzoff ED. 1988. Probing enzyme–substrate recognition and catalytic mechanism in Cu,Zn superoxide dismutase. In: Simic MG, Taylor KA, Ward JF, Sontag CV, eds. *Oxygen radicals in biology and medicine*. New York: Plenum Press. pp 635–640.

Valentine JS, Pantoliano MW. 1981. Protein-metal ion interactions in cuprozinc protein (superoxide dismutase): A major intracellular repository for copper and zinc in the eukaryotic cell. In: Spiro TG, ed. *Copper proteins*. New York: John Wiley and Sons, Inc. pp 292–358.

Wiedau-Pazos M, Goto JJ, Rabizadeh S, Gralla EB, Roe JA, Lee MK, Valentine JS, Bredesen DE. 1996. Altered reactivity of superoxide dismutase in familial amyotrophic lateral sclerosis. *Science 271*:515–518.

Wong PC, Pardo CA, Borchelt DR, Lee MK, Copeland NG, Jenkins NA, Sisodia SS, Cleveland DW, Price DL. 1995. An adverse property of a familial ALS-linked SOD1 mutation causes motor neuron disease characterized by vacuolar degeneration of mitochondria. *Neuron 14*:1105–1116.

Yim HS, Kang JH, Chock PB, Stadtman ER, Yim MB. 1997. A familial amyotrophic lateral sclerosis-associated A4V Cu,Zn-superoxide dismutase mutant has a lower K_m for hydrogen peroxide. Correlation between clinical severity and the K_m value. *J Biol Chem 272*:8861–8863.

Yim MB, Kang JH, Yim HS, Kwak HS, Chock PB, Stadtman ER. 1996. A gain-of-function of an amyotrophic lateral sclerosis-associated Cu,Zn-superoxide dismutase mutant: An enhancement of free radical formation due to a decrease in K_m for hydrogen peroxide. *Proc Natl Acad Sci USA 93*:5709–5714.